

Article

Development of a Model to Estimate the Thermodynamic Stability of Organic Substances in Leaching Processes

Carlos Ocampo-López ^{1,*}, Álvaro Ospina-Sanjuan ², Margarita Ramírez-Carmona ¹ and Leidy Rendón-Castrillón ¹

¹ Faculty of Chemical Engineering, Centro de Estudios y de Investigación en Biotecnología (CIBIOT), Universidad Pontificia Bolivariana, Circular 1A No. 70-01, Bloque 11, Medellín 050031, Colombia

² Faculty of Electric and Electronic Engineering, Grupo de Investigaciones en Bioingeniería y Microelectrónica, Universidad Pontificia Bolivariana, Circular 1A No. 70-01, Bloque 11, Medellín 050031, Colombia

* Correspondence: carlos.ocampo@upb.edu.co

Abstract: The leaching processes for metals using organic substances represent a sustainable approach to recover precious minerals from solid matrices. However, the generation of organometallic species and the lack of thermodynamic diagrams make it difficult to advance the understanding of their behavior and optimize the process. In this work, a thermodynamically and stoichiometrically consistent mathematical model was developed to estimate the thermodynamic stability of organic substances during the leaching process, and iron leaching with oxalic acid was used as a case study. The Pourbaix and the global thermodynamic stability diagrams for the system were developed in this study. Using a Gaussian[®], it was estimated that the Gibbs free energy formation for $\text{Fe}(\text{C}_2\text{O}_4)_2^{2-}$, $\text{Fe}(\text{C}_2\text{O}_4)_2^{1-}$, and $\text{Fe}(\text{C}_2\text{O}_4)_3^{3-}$ was -1407.51 , -2308.38 , and -3068.89 kcal/mol. A set of eleven independent reactions was formulated for the sixteen species involved in the leaching process, and its stability functions in terms of E_h and pH were calculated to generate a 3D global thermodynamic stability diagram. According to the E_h -pH diagrams for the leaching process, ferrioxalate was identified as the most stable and predominant species in the leaching process at pH above 6.6 under reductive conditions. The mathematical model developed in this work resulted in a thermodynamic tool for predicting leaching processes.

Keywords: organic leaching; E_h -pH diagrams; stability; Pourbaix; iron; free energy; oxalates; 3D E_h -pH diagrams



Citation: Ocampo-López, C.; Ospina-Sanjuan, Á.; Ramírez-Carmona, M.; Rendón-Castrillón, L. Development of a Model to Estimate the Thermodynamic Stability of Organic Substances in Leaching Processes. *Metals* **2022**, *12*, 1424. <https://doi.org/10.3390/met12091424>

Academic Editors: Chen Tian, Xu Yan and Zhang Lin

Received: 25 July 2022

Accepted: 24 August 2022

Published: 28 August 2022

Publisher's Note: MDPI stays neutral with regard to jurisdictional claims in published maps and institutional affiliations.



Copyright: © 2022 by the authors. Licensee MDPI, Basel, Switzerland. This article is an open access article distributed under the terms and conditions of the Creative Commons Attribution (CC BY) license (<https://creativecommons.org/licenses/by/4.0/>).

1. Introduction

Metal resources are found in complex and low-grade ores, in old waste deposits related to mining work sites [1], and in other sources such as electronic waste, which generates between 20 and 50 million tons per year worldwide, with an average annual growth rate of 3% to 5%, three times higher than that of other solid waste [2]. Likewise, it is estimated that, each year, more than 10 billion tons of mining tailings are produced worldwide [3].

Adopting a sustainable approach to the circular economy system and evaluating that the production of materials from primary sources has more negative environmental impacts than secondary sources [4], the scarcity of natural resources leads to a projection of the closure of approximately 15 Chilean hydrometallurgical plants before 2030 [5]. The recovery of metals from residual solid matrices is proposed as an alternative through leaching processes. These can be defined as the selective removal and extraction of metal species from an ore or solid matrix, caused by allowing a suitable leaching agent solvent to percolate into and through the matrix containing the metal values. Leaching is used in metallurgy and frequently extracts minerals such as gold, silver, and copper at an industrial level [1].

Numerous studies have been conducted on the leaching of metals from solid matrices, such as minerals, ashes, e-waste, and batteries, using organic acids. The most common

organic lixivants are oxalic acid, citric acid, DL-malic acid, tartaric acid, succinic acid, formic acid, lactic acid, and aspartic acid [6].

The mobilization and leaching of metals from solid matrices by organic acids are based mainly on two mechanisms, acidolysis and complexolysis. In acidolysis, solubilization occurs via metal protonation of the species on the solid matrix surface. During acidolysis, the acid dissociates and releases the protons. The protons (H^+) protonate the anion of the insoluble metal compounds, and the metal is detached from the surface. In complexation, organic acids create ligands with the leached metal and form soluble metal complexes with different stabilities depending on the organic acid structure. If the ligand formed is stable, the probabilities of adsorption and reversibility of the metal into the solid matrix are reduced, and the leaching is more favorable [7].

In the case of iron leaching from kaolin clay with oxalic acid ($H_2C_2O_4$), the first step of the oxidation occurs when the H^+ ions of the oxidizing agent are deposited on the surface of iron oxides ($>FeIII-O$), forming active sites ($>FeIII-OH$) in the kaolin particle [8]. The second step occurs when a ligand complex of oxalate (L^{-n}) is deposited on the sites previously activated in the first step. The third step is called non-reductive dissolution, which consists of a simple process of desorption of the ferric ions adsorbed on the surface ($[>FeIII-L]^{-(n-2)}$) and their transfer to the acid solution. The nonreductive dissolution mechanism removes only the most reactive sites on the oxide surface as a stable oxalate species. The number of active sites increases with decreasing pH and increasing temperature [8,9].

The computational prediction and evaluation of the performance of a process towards its optimization require a mathematical model that represents the consumption, production, and species stability. There is a lack of understanding of many of the chemical phenomena that take place, increasing the difficulty of predicting the effect of process alterations on the required processing time and product composition [10]. Studies support decision-making based on knowledge to manage the operating mode of the leaching process, fundamentally supported by the phenomenological behavior of the chemical system, from which operational conditions are derived at the macroscopic level [11].

Likewise, Saldaña et al. developed a method to model, sensitize, and optimize mineral recovery in cells using a discrete event simulation framework and analytical model tuning, based on operational data from a mineral concentration pilot plant. The incorporation of the characterization of the matrix and its chemical behavior could strengthen machine-learning models to control the process [12].

To overcome some of the difficulties and ambiguities of the standard thermodynamic description of complex chemical systems, Fishtik proposed methodologies for the thermodynamic coupling of chemical reactions, showing that the fundamental equations of chemical thermodynamics may be reformulated in terms of a particular class of chemical reactions, called response reactions (RERs), using a matrix approach. This methodology could expand the quantitative and qualitative knowledge of intricate systems, such as organometallic species involved in mineral processing.

In the design and operation of mineral beneficiation processes, such as leaching, in which oxidation–reduction reactions, acid–base reactions, ligand formation, temperature, or pressure occur, it is necessary to have Pourbaix or E_h -thermodynamic diagrams: pH, where E_h represents the oxidation–reduction potential based on the standard hydrogen potential, while pH represents the activity of the hydrogen ion [13].

The most widely used acids in leaching processes on an industrial scale are sulfuric and phosphoric acid. Other authors report experimental studies of mineral removal where organic acids, such as oxalic acid and ascorbic acid [10,14] are used. It is considered that oxalic acid has a higher potential for the removal of mineral species, given its complexing behavior and its selectivity [15].

The thermodynamic aspects of leaching have been studied in a limited way and are commonly applied to ideal conditions since there are no reference data for the calculation of the global stabilities of the species involved in the process and the number of physicochemical interactions that occur between process variables [16,17].

Pourbaix diagrams are used to simplify the analysis and generate a rapid understanding of the behavior of leaching systems in solid matrices [18], which can be constructed theoretically by calculating the global stability, as exposed by Fishtik [19–21].

In the literature, authors such as Schmidt et al. [22], Fishtik [19], and Panias [23] proposed a matrix methodology for the thermodynamic analysis of metal species using a matrix analysis based on the concept of the general stability of chemical species in multiple chemical reaction systems. However, no results were reported for organic or organometallic species in the leaching processes.

Therefore, in this study, a mathematical model was developed to estimate the thermodynamic stability of organic substances in leaching processes, allowing the generation of Pourbaix diagrams to establish adequate operational conditions, optimize the recovery of metals from solid matrices, and find the species more stable in each set of operating conditions used.

2. Materials and Methods

2.1. Obtention of the Independent Reaction System for the Leaching Process

The concept of global stability of the species was used to construct the Pourbaix diagram (E_h -pH), according to the methodology proposed by [19]. In the first stage, a set of independent stoichiometric reactions representing the redox behavior of the system was formulated from the species involved, adding the three species that participated in the reactions: electrons (e^-), H^+ (aq), and H_2O (l). An ideal aqueous solution was assumed for the ionic species.

To obtain the set of independent reactions, the stepwise reduction matrix method in the atomic matrix proposed by Recklaitis [24] was used, in which e^- , H, O, Fe, and $C_2O_4^{2-}$ were taken as reference “elements”. For this study, an “element” is a molecular or ionic species that makes up one of the species involved in the reaction system.

A system formed by n species in the liquid or solid phase B_i ($i = 1, 2, \dots, n$) was considered, where each species has an activity coefficient a_i ($i = 1, 2, \dots, n$). A fixed temperature of 25 °C and a constant pressure of 101.3 kPa were taken as references. \bar{G}_i (T, P, a_1, \dots, a_n) was defined as the partial Gibbs free energy of the species. If the matrix element ϵ_{ij} ($i = 1, \dots, n; j = 1, \dots, s$) is defined as the number of elements E_j ($j = 1, \dots, s$) in the species B_i , the following vectors are generated:

$$B = (B_1, B_2, \dots, B_n)^T \quad (1)$$

$$E = (E_1, E_2, \dots, E_n)^T \quad (2)$$

$$\bar{G} = (\bar{G}_1, \bar{G}_2, \dots, \bar{G}_n)^2 \quad (3)$$

where $B = \epsilon E$. $\rho = \nu B = 0$ is defined as a vector of independent chemical reactions formed by the linear combination of a matrix of stoichiometric coefficients ν , of dimensions $n \times m$, and the vector of species B , as previously described, in such a way that: $\rho = (\rho_1, \rho_2, \dots, \rho_m)^T$, where m represents the number of independent chemical reactions between the species of the system.

2.2. Gibbs Free Energy of Formation Calculations

Calculations of the Gibbs free energy of formation for the aqueous oxalate species $Fe(C_2O_4)_2^{2-}$, $Fe(C_2O_4)_2^{1-}$, and $Fe(C_2O_4)_3^{3-}$ were performed with Gaussian 09. The energies of the studied compounds were calculated using two theoretical methods of Gaussian-n model chemistry at the G3 [25] and G4 [26] levels. The energies were calculated by G3 and G4 at 0 K.

To execute the Gaussian calculation routines, the program was administered to the SGE manager of the distributed computing resources so that these resources were used in the most efficient way by a group of users in a computing cluster [27].

2.3. Obtention of the Pourbaix Diagram

Using the concepts of chemical thermodynamics, the changes in free energy of a thermodynamic system with chemical reactions were evaluated using the expression:

$$\Delta G = \nu \bar{G} \quad (4)$$

where, for each reaction ρ_m , the Gibbs free energy change was given by:

$$\Delta G_j = \Delta G_j^0(T, P) + RT \ln \prod_{i=1}^n a_i^{\nu_{ij}} = 0; \quad (5)$$

which is an implicit function of the pH and the oxidation–reduction potential E_h , given the functional relationship of the activity coefficient with the H^+ ions and the electrons transferred during the progress of all of the reactions ρ_m .

The global thermodynamic stability was defined, for each substance involved in the process, as a vector of n components of the form:

$$\Sigma = \nu^T (\nu \nu^T)^{-1} \Delta G. \quad (6)$$

where

$$\Sigma = \Sigma(T, P, \text{pH}, E_h) \quad (7)$$

The pH and E_h values that minimized the vector of global stabilities of the species (Σ), representing points of thermodynamic stability, which are plotted on a plane, were allowed to establish the stability regions, generating a stability diagram for a leaching process. The species with the lowest overall stability is the dominant species

To gather the set of points, a MATLAB routine was programmed. The calculation routines comprised 3 phases, which included: creating an independent stoichiometric system from the substances to be evaluated in the thermodynamic study; calculating the global thermodynamic stability functions using symbolic variables; and evaluating the coordinates of the triple points and the lines of the Pourbaix diagram through combinatory cycles by minimizing the stability functions of the substances to be evaluated. Finally, with the data found, the Pourbaix diagram was elaborated.

3. Results and Discussions

Pourbaix diagrams were used to evaluate the regions of the stability of materials subjected to different conditions from potential and pH in aqueous environments. However, the exploration of leaching processes and the increasing complexity of chemical systems pose challenges in performing thermodynamic analysis in multidimensional systems [28].

In this study, the leaching of minerals from iron species in the presence of oxalic acid as an organic leaching agent was taken as a case study. During the leaching process, a set of complex organometallic species, such as $\text{Fe}(\text{C}_2\text{O}_4)_2^{2-}$, $\text{Fe}(\text{C}_2\text{O}_4)_2^{1-}$, and $\text{Fe}(\text{C}_2\text{O}_4)_3^{3-}$ are formed, since oxalic acid is a complexing agent with metallic species. These iron oxalates have different degrees of stability depending on their chemical structure, sometimes generating reversibility processes that result in iron deposition on the surface of the ore during the leaching processes [9,29,30]. Since this fact is undesirable, it is desirable that the leaching favors the formation of stable organometallic compounds in an aqueous solution, which allows the effective removal of metallic species. There is no Pourbaix diagram for the iron–oxalic acid–water system in the reviewed literature, nor are there complete thermodynamic data on its Gibbs energies of formation [8,31].

Although other species of oxalates can be formed with the iron atom during the acidolysis and complexation stages, a previous doctoral study [32] found that the $\text{Fe}(\text{C}_2\text{O}_4)_2^{2-}$, $\text{Fe}(\text{C}_2\text{O}_4)_2^{1-}$, and $\text{Fe}(\text{C}_2\text{O}_4)_3^{3-}$ species are the most stable and the most abundant during the leaching processes. This evidence was confirmed in other scientific studies, in which similar results were found using photolysis techniques [31,33].

3.1. Gibbs Free Energy of Formation of Species

One of the limitations of carrying out studies on thermodynamic stability in systems of multiple species is the estimation of the Gibbs energies of formation of each one. Although there are handbooks that consolidate the thermodynamic data of the best-known species, some of the molecules, especially organometallic ones, do not have data available; therefore, they must be estimated using computational calculations by software such as Gaussian.

The Gibbs free energy of formation for $\text{Fe}(\text{C}_2\text{O}_4)_2^{2-}$, $\text{Fe}(\text{C}_2\text{O}_4)_2^{1-}$, and $\text{Fe}(\text{C}_2\text{O}_4)_3^{3-}$ was estimated using Gaussian 09 software (Gaussian, Inc., Wallingford, CT, USA), as shown in Table 1.

Table 1. List of Gibbs free energies of formation for the calculation of thermodynamic stabilities.

Species	ΔG_f° (kcal/mol)	Source
Fe	0.00	[19,34]
Fe^{2+}	−21.88	[35]
Fe^{3+}	−4.11	[19]
FeC_2O_4	−1407.51	[14,32]
$\text{Fe}(\text{C}_2\text{O}_4)_2^{2-}$	−2308.38	This study
$\text{Fe}(\text{C}_2\text{O}_4)_2^{1-}$	−3068.89	This study
$\text{Fe}(\text{C}_2\text{O}_4)_3^{3-}$	−3753.88	This study
FeOOH	−117.07	[19]
$\text{Fe}(\text{OH})_2$	−116.39	[36]
Fe_3O_4	−242.65	[36]
$\text{C}_2\text{O}_4^{2-}$	+7281.06	[36]
HC_2O_4^-	+1541.17	[35]
$\text{H}_2\text{C}_2\text{O}_4$	−166.52	[35]
e^-	0.00	[19]
H^+	0.00	[19]
H_2O	−56.58	[35]

3.2. Independent Reaction System Estimation

The Pourbaix analysis was limited to three or fewer elements in previous studies found in the literature, largely because calculating the electrochemical phase stability of higher composition spaces was proved to be inefficient with existing methods [28]. Two different approaches may be used to construct an E_h -pH diagram. One is to calculate the equilibrium equations manually between pairs of species and to construct the diagram by plotting the resulting equilibrium lines. The other is to perform the equilibrium calculations from all of the involved species at each point in a grid then to select the predominant species at each point [13].

The methodology used in this study spends only 4.5 min to calculate the species stability and estimate the E_h -pH diagram for 16 species and involves the creation of an independent reaction system from an atomic matrix using a linear algebra approach [24]. The formulation of the atomic matrix is shown in Table 2. It consists of an arrangement in which the species involved in the system are found in rows and the reference elements in columns.

In this matrix arrangement, chemical species are usually represented as an inventory of the chemical elements that compose them. Since, in this case, the oxalate ions are not degraded to simpler molecules or even their atoms, they were taken as a reference, assuming that they fulfill the same role as a chemical element. Fishtik suggested this simplification in his research on thermodynamic stability [20].

Table 3 shows the independent reaction matrix obtained for the iron–oxalic acid–water system used as a case study. Eleven independent reactions were obtained after performing a matrix reduction process of the atomic matrix using the Matlab software (Matlab R12, MathWorks, Natick, MA, USA). These reactions explain the stoichiometry of the leaching process and serve as the basis for the formulation of thermodynamic stability functions for each species.

Table 2. Atomic matrix formulated for the leaching-related species. In the columns, e^- , H, O, Fe, and $C_2O_4^{2-}$ were taken as reference elements.

Species	B_i	e^-	H	O	Fe	$C_2O_4^{2-}$
Fe	1	1	0	0	0	0
Fe^{2+}	2	-1	1	0	0	0
Fe^{3+}	3	0	2	1	0	0
FeC_2O_4	4	0	0	0	1	0
$Fe(C_2O_4)_2^{2-}$	5	0	2	0	0	1
$Fe(C_2O_4)_2^{1-}$	6	-2	0	0	1	0
$Fe(C_2O_4)_3^{3-}$	7	-3	0	0	1	0
FeOOH	8	0	0	0	1	1
$Fe(OH)_2$	9	2	0	0	1	2
Fe_3O_4	10	1	0	0	1	2
$C_2O_4^{2-}$	11	3	0	0	1	3
$HC_2O_4^-$	12	0	1	2	1	0
$H_2C_2O_4$	13	0	2	2	1	0
e^-	14	0	0	4	3	0
H^+	15	2	0	0	0	1
H_2O	16	1	1	0	0	1

Table 3. Independent reaction matrix (ν) obtained for the iron–oxalic acid–water system.

ν	B_1	B_2	B_3	B_4	B_5	B_6	B_7	B_8	B_9	B_{10}	B_{11}	B_{12}	B_{13}
ρ_1	-1	1	0	0	0	0	0	0	0	0	0	0	0
ρ_2	-1	0	1	0	0	0	0	0	0	0	0	0	0
ρ_3	-1	0	0	1	0	0	0	0	0	0	0	0	-1
ρ_4	-1	0	0	0	1	0	0	0	0	0	0	0	-2
ρ_5	-1	0	0	0	0	1	0	0	0	0	0	0	-2
ρ_6	-1	0	0	0	0	0	1	0	0	0	0	0	-3
ρ_7	-1	0	0	0	0	0	0	1	0	0	0	0	0
ρ_8	-1	0	0	0	0	0	0	0	1	0	0	0	0
ρ_9	-3	0	0	0	0	0	0	0	0	1	0	0	0
ρ_{10}	0	0	0	0	0	0	0	0	0	0	1	0	-1
ρ_{11}	0	0	0	0	0	0	0	0	0	0	0	1	-1

In each row from Table 3, a negative value represents the stoichiometric coefficient of a reactant, and a positive one the coefficient of a product. Table 4 summarizes the stoichiometric representation of the eleven independent reactions for the iron–oxalic acid–water system.

Table 4. Stoichiometric representation of the eleven independent reactions for the iron–oxalic acid–water system.

Independent Reaction	Stoichiometric Reaction
ρ_1	$Fe \rightarrow Fe^{+2} + 2e^-$
ρ_2	$Fe \rightarrow Fe^{+3} + 3e^-$
ρ_3	$Fe^{+2} + C_2O_4^{2-} \rightarrow FeC_2O_4$
ρ_4	$Fe^{+2} + 2C_2O_4^{2-} \rightarrow Fe(C_2O_4)_2^{2-}$
ρ_5	$Fe^{+3} + 2C_2O_4^{2-} \rightarrow Fe(C_2O_4)_2^{1-}$
ρ_6	$Fe^{+3} + 3C_2O_4^{2-} \rightarrow Fe(C_2O_4)_3^{3-}$
ρ_7	$Fe + 2H_2O \rightarrow FeOOH + 3H^+ + 3e^-$
ρ_8	$Fe + 2H_2O \rightarrow Fe(OH)_2 + 2H^+ + 2e^-$
ρ_9	$3Fe + 4H_2O \rightarrow Fe_3O_4 + 8H^+ + 8e^-$
ρ_{10}	$H_2C_2O_4 \rightarrow H^+ + HC_2O_4^-$
ρ_{11}	$HC_2O_4^- \rightarrow H^+ + C_2O_4^{2-}$

These independent reactions explain the formation or the interaction of each species involved in the process. For example, reactions 1–2 explain the speciation of iron as redox reactions, reactions 3–6 explain the reactions between iron species and oxalate to generate multiple iron oxalate complexes, reactions 7–9 explain the oxidation reactions of iron to generate oxides and hydroxides, and reactions 10–11 represent the oxalic acid dissolution. The reactions coincide with the previous results found in the reviewed literature. However, when expressing a purely stoichiometric and independent system, it is not necessary that the eleven reactions coincide with the reaction mechanisms that occur in the experimental reality of this process since the changes in free energy will be the same, given the law of conservation of matter [9,31,37].

3.3. Stability Functions and Pourbaix Diagrams

For each species, the global thermodynamic stability (Σ_i) was calculated as a function of the pH and the redox potential E_h , using the software developed in MATLAB and applying the matrix expression shown in Equation (6). The stability functions obtained for the system are listed in Equations (8)–(20):

$$\Sigma_1 = 0.1167(\text{pH}) + 2.3964(E_h) + 4.5059 \quad (8)$$

$$\Sigma_2 = 0.1167(\text{pH}) + 0.3964(E_h) + 3.5571 \quad (9)$$

$$\Sigma_3 = 0.1167(\text{pH}) - 0.6036(E_h) + 4.3276 \quad (10)$$

$$\Sigma_4 = 0.0615(\text{pH}) + 0.5200(E_h) - 2.3316 \quad (11)$$

$$\Sigma_5 = 0.0615(\text{pH}) + 0.5200(E_h) - 41.3973 \quad (12)$$

$$\Sigma_6 = 0.0062(\text{pH}) - 0.3564(E_h) - 20.1779 \quad (13)$$

$$\Sigma_7 = -0.0490(\text{pH}) - 0.2327(E_h) + 4.3163 \quad (14)$$

$$\Sigma_8 = -0.0606(\text{pH}) - 0.6036(E_h) + 4.3450 \quad (15)$$

$$\Sigma_9 = -0.0015(\text{pH}) + 0.3964(E_h) + 4.3745 \quad (16)$$

$$\Sigma_{10} = -0.1227(\text{pH}) - 0.8109(E_h) + 12.8268 \quad (17)$$

$$\Sigma_{11} = -0.0552(\text{pH}) + 0.1236(E_h) + 23.9049 \quad (18)$$

$$\Sigma_{12} = 0.0039(\text{pH}) + 0.1236(E_h) + 23.6525 \quad (19)$$

$$\Sigma_{13} = 0.0630(\text{pH}) + 0.1236(E_h) + 23.5784 \quad (20)$$

These stability functions, understood as scalar fields, make up a set of three-dimensional planes whose intersections define stability regions and boundaries of an E_h -pH diagram. The intersection of two planes represents a boundary line as a function of E_h and pH variables, and the simultaneity of the three planes indicates a point on a 2D display of a Pourbaix diagram.

Using a species combinatorics' algorithm two by two and three by three, it was possible to obtain the triple points and boundaries of the E_h -pH diagram for the iron–oxalic acid–water system using a calculation routine in the MATLAB software. The points that generated a solution in the domain of real numbers are shown in Figure 1.

According to the Pourbaix diagram, the stability regions include metallic iron (Fe), oxidized iron species (Fe^{+2} , Fe^{+3}), goethite (FeOOH), and only one of the three iron oxalates, namely, ferrioxalate, $\text{Fe}(\text{C}_2\text{O}_4)_3^{3-}$.

Along with the stability boundaries between the species, the numerical value of the global stability is shown in colors. It was found that for leaching processes at acidic pH and under oxidative conditions, Fe^{+2} is the most stable species. When the leaching pH alkalizes and approaches values above 6.6, the ferrioxalate species becomes more stable and predominant in the system. It subsequently complexes the iron into a thermodynamically stable structure.

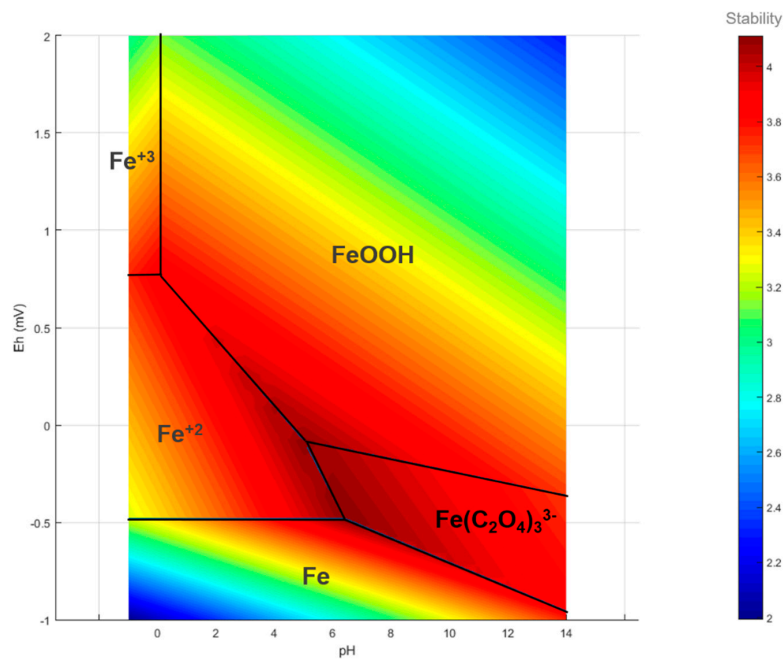


Figure 1. The Pourbaix diagram obtained for the iron–oxalic acid–water system at 25 °C and 101.3 kPa.

Studies reported by [29], in which iron species removal processes were performed in kaolin, suggest that at concentrations of Fe^{+3} greater than 10^{-6} M, an iron complex is exclusively formed. The Fe^{+3} oxalate complexes are more stable than the Fe^{+2} complexes according to the order of magnitude of their respective formation energies. This fact was verified by [8], who verified this fact through equilibrium-constant calculations and found that the dissociation constant is 3×10^{-21} and that of 2×10^{-8} .

Figure 2 shows the 3D surface of the global thermodynamic stability diagram obtained for the iron–oxalic acid–water system at 25 °C and 101.3 kPa as a function of E_h and pH.

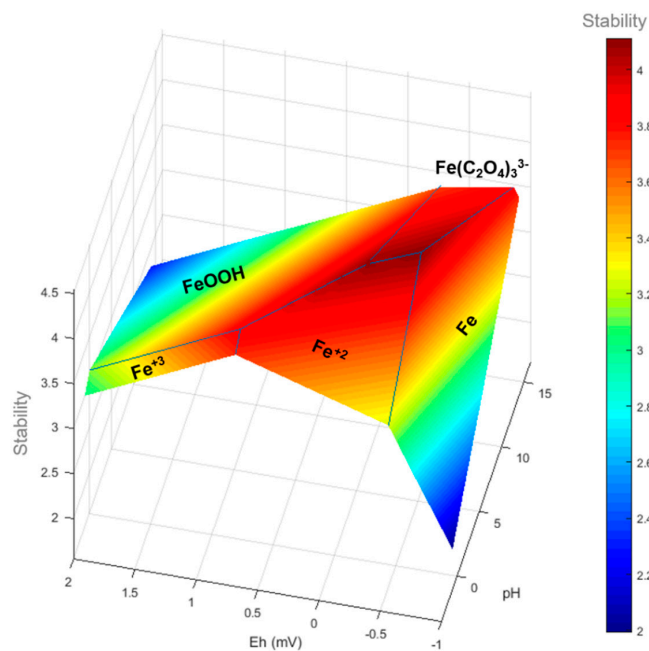


Figure 2. Global thermodynamic stability diagram obtained for the iron–oxalic acid–water system at 25 °C and 101.3 kPa.

The topology of the global thermodynamic stability diagram shows how the species become predominant at specific E_h and pH during the leaching process. The overall stable species is ferrioxalate, followed by Fe^{+2} . On a 3D overall Pourbaix diagram, only the planes with the lowest value of the overall stability should be present.

The ferrioxalate molecule is described in Figure 3. One of the explanations for its stability is the orientation of the oxalate coordination around the iron atom. The repulsion of oxygen atoms locates the oxalate bonds symmetrically, and the iron center in the ferrioxalate anion has a distorted octahedral geometry. If compared with other iron oxalates, such as $Fe(C_2O_4)_2^{2-}$ and $Fe(C_2O_4)_3^{1-}$, the Gibbs free energy of formation for ferrioxalate was estimated as the lowest, which demonstrates its further thermodynamic stability. In the absence of light or other radiation, the ferrioxalate complex is quite stable

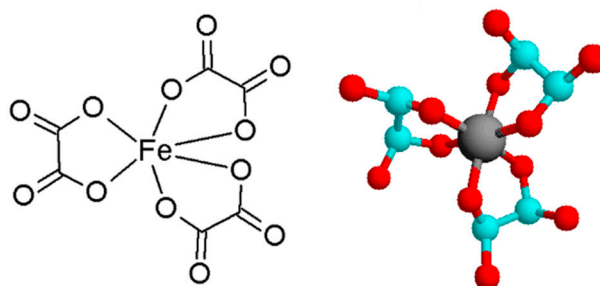


Figure 3. Representation of the ferrioxalate molecule found as the most stable species in the leaching system iron–oxalic acid–water. 2D (left) and 3D (right).

According to the mathematical model developed in this article, the overall stability of the species may be considered as an exact, complete, and unique thermodynamic and stoichiometric balance in the system. Calculating the global stabilities of the species as a function of the pH and the redox potential E_h , as well as the global stability diagram, represents a thermodynamic tool for predicting the leaching processes. This tool establishes the practical limits of the leaching processes and consequently allows for optimizing the operative variables or defining the control points during automation on an industrial scale.

Although the leaching processes are a crucial stage in metal recovery processes, the techniques adopted are somewhat empirical, and only a few works have analyzed the processes from a thermodynamic point of view before their implementation. This work provides a thermodynamic approach for developing efficient processes and reduces the consumption of resources used in research, which benefits future research in practical applications.

Pourbaix diagrams are a valuable tool for exploring the corrosion profiles of materials as a function of ambient pH and electrochemical potential (E_h). In multicomponent systems, these diagrams serve as a tool to assess the chemical behavior of catalysts in mining processes to predict the ease or operational conditions of leaching processes. However, Pourbaix analysis was limited to three or fewer elements, largely because calculating the electrochemical phase stability of higher composition spaces was proved to be ineffective with the traditional methods reported in the literature [28].

4. Conclusions

In this work, a model was developed to estimate the thermodynamic stability of organic substances in leaching processes, and iron leaching with oxalic acid was used as a case study. The Pourbaix and the global thermodynamic stability diagrams for the iron–oxalic acid–water system that were not previously reported in the literature were developed in this study. Using computational calculations, it was possible to estimate the Gibbs free energy of formation for $Fe(C_2O_4)_2^{2-}$, $Fe(C_2O_4)_2^{1-}$, and $Fe(C_2O_4)_3^{3-}$ as -1407.51 , -2308.38 , and -3068.89 kcal/mol. A set of eleven independent reactions was formulated for the sixteen species involved in the leaching process, and its stability functions in terms

of E_h and pH were calculated to generate a 3D global thermodynamic stability diagram. According to the E_h -pH diagrams for the leaching process, ferrioxalate was identified as the most stable and predominant species in the leaching process at a pH above 6.6 and reductive conditions ($E_h < 0$). The mathematical model developed in this work resulted in a thermodynamic tool for predicting leaching processes, with a particular focus on organometallic species where organic acids are used as the leachate agents.

Author Contributions: Conceptualization, C.O.-L., Á.O.-S., M.R.-C., and L.R.-C.; methodology, C.O.-L.; software, C.O.-L. and Á.O.-S.; validation, C.O.-L., Á.O.-S., M.R.-C., and L.R.-C.; formal analysis, C.O.-L., Á.O.-S., M.R.-C., and L.R.-C.; investigation, C.O.-L., Á.O.-S., M.R.-C., and L.R.-C.; resources, C.O.-L. and Á.O.-S.; data curation, C.O.-L., Á.O.-S., M.R.-C., and L.R.-C.; writing—original draft preparation, C.O.-L., Á.O.-S., M.R.-C., and L.R.-C.; writing—review and editing, C.O.-L., Á.O.-S., M.R.-C., and L.R.-C.; visualization, C.O.-L. and L.R.-C.; supervision, C.O.-L.; project administration, C.O.-L.; funding acquisition, C.O.-L., Á.O.-S., and M.R.-C. All authors have read and agreed to the published version of the manuscript.

Funding: The APC was funded by Universidad Pontificia Bolivariana. No external funding was received.

Institutional Review Board Statement: Not applicable.

Informed Consent Statement: Not applicable.

Data Availability Statement: Not applicable.

Conflicts of Interest: The authors declare no conflict of interest.

References

1. Saldaña, M.; Gálvez, E.; Robles, P.; Castillo, J.; Toro, N. Copper Mineral Leaching Mathematical Models—A Review. *Materials* **2022**, *15*, 1757. [[CrossRef](#)] [[PubMed](#)]
2. Wen, X.; Wang, J.; Wang, H. Research on the Mathematical Model of Local Equilibrium in the Top-Blown Smelting Process of Electronic Waste. *Metals* **2021**, *11*, 1500. [[CrossRef](#)]
3. Wang, G.; Xiao, H.; Liang, G.; Zhu, J.; He, C.; Ma, S.; Shuai, Z.; Komarneni, S. Leaching Characteristics and Stabilization of Heavy Metals in Tin-Polymetallic Tailings by Sodium Diethyl Dithiocarbamate Intercalated Montmorillonite (DDTC-Mt). *J. Clean. Prod.* **2022**, *344*, 131041. [[CrossRef](#)]
4. Yuksekdag, A.; Kose-Mutlu, B.; Siddiqui, A.F.; Wiesner, M.R.; Koyuncu, I. A Holistic Approach for the Recovery of Rare Earth Elements and Scandium from Secondary Sources under a Circular Economy Framework—A Review. *Chemosphere* **2022**, *293*, 133620. [[CrossRef](#)] [[PubMed](#)]
5. Moraga, G.A.; Jamett, N.E.; Hernández, P.C.; Graber, T.A.; Taboada, M.E. Chalcopyrite Leaching with Hydrogen Peroxide and Iodine Species in Acidic Chloride Media at Room Temperature: Technical and Economic Evaluation. *Metals* **2021**, *11*, 1567. [[CrossRef](#)]
6. Musariri, B.; Akdogan, G.; Dorfling, C.; Bradshaw, S. Evaluating Organic Acids as Alternative Leaching Reagents for Metal Recovery from Lithium Ion Batteries. *Miner. Eng.* **2019**, *137*, 108–117. [[CrossRef](#)]
7. Pathak, A.; Vinoba, M.; Kothari, R. Emerging Role of Organic Acids in Leaching of Valuable Metals from Refinery-Spent Hydroprocessing Catalysts, and Potential Techno-Economic Challenges: A Review. *Crit. Rev. Environ. Sci. Technol.* **2021**, *51*, 1–43. [[CrossRef](#)]
8. Pnias, D. Mechanisms of Dissolution of Iron Oxides in Aqueous Oxalic Acid Solutions. *Hydrometallurgy* **1996**, *42*, 257–265. [[CrossRef](#)]
9. Lee, S.; Tran, T.; Jung, B.; Kim, S.; Kim, M. Dissolution of Iron Oxide Using Oxalic Acid. *Hydrometallurgy* **2007**, *87*, 91–99. [[CrossRef](#)]
10. Rendón-Castrillón, L.; Ramírez-Carmona, M.; Ocampo-López, C.; Gómez-Arroyave, L. Mathematical Model for Scaling up Bioprocesses Using Experiment Design Combined with Buckingham Pi Theorem. *Appl. Sci.* **2021**, *11*, 11338. [[CrossRef](#)]
11. Saldaña, M.; Neira, P.; Flores, V.; Robles, P.; Moraga, C. A Decision Support System for Changes in Operation Modes of the Copper Heap Leaching Process. *Metals* **2021**, *11*, 1025. [[CrossRef](#)]
12. Saldaña, M.; Neira, P.; Flores, V.; Moraga, C.; Robles, P.; Salazar, I. Analysis of the Dynamics of Rougher Cells on the Basis of Phenomenological Models and Discrete Event Simulation Framework. *Metals* **2021**, *11*, 1454. [[CrossRef](#)]
13. Huang, H.H. The Eh-PH Diagram and Its Advances. *Metals* **2016**, *6*, 23. [[CrossRef](#)]
14. Ocampo-López, C.; Ramírez-Carmona, M.E.; Vélez-Ortiz, E. Thermodynamic Analysis of Stability in Iron Removal from Kaolin by Using Oxalic Acid. *Ceramica* **2013**, *59*, 326–330. [[CrossRef](#)]
15. Ramírez-Carmona, M.; Rendon-Castrillon, L.; Ocampo-López, C.; Giraldo-Aristizabal, R. Proceso Para la Separación de Metales en una Matriz Sólida Mediante Lixiviación, Que Emplea una Composición Que Contiene Ácidos Carboxílicos, Monosacáridos, Disacáridos, Aminoácidos, Ácidos Grasos, Alcoholes y Compuestos Fenólicos. Patent Number NC2019/0013648, 2022. 13.

16. Bhattacharyya, K.G.; Gupta, S. Adsorption of a Few Heavy Metals on Natural and Modified Kaolinite and Montmorillonite: A Review. *Adv. Colloid Interface Sci.* **2008**, *140*, 114–131. [[CrossRef](#)]
17. Jiang, M.; Wang, Q.; Jin, X.; Chen, Z. Removal of Pb(II) from Aqueous Solution Using Modified and Unmodified Kaolinite Clay. *J. Hazard. Mater.* **2009**, *170*, 332–339. [[CrossRef](#)]
18. Ippolito, N.M.; Medici, F.; Pietrelli, L.; Piga, L. Effect of Acid Leaching Pre-Treatment on Gold Extraction from Printed Circuit Boards of Spent Mobile Phones. *Materials* **2021**, *14*, 362. [[CrossRef](#)]
19. Fishtik, I. Thermodynamic Stability Relations in Redox Systems. *Environ. Sci. Technol.* **2006**, *40*, 1902–1910. [[CrossRef](#)]
20. Fishtik, I. Thermodynamic Stability of Chemical Species in Multiple Reaction Systems. *J. Phys. Chem. B* **2005**, *109*, 3851–3859. [[CrossRef](#)]
21. Fishtik, I.; Datta, R. A General Thermodynamic and Stoichiometric Theory of Stability of Chemical Species. *Society* **2004**, *108*, 5727–5739. [[CrossRef](#)]
22. Schmidt, J.; Shi, J.; Borlido, P.; Chen, L.; Botti, S.; Marques, M.A.L. Predicting the Thermodynamic Stability of Solids Combining Density Functional Theory and Machine Learning. *Chem. Mater.* **2017**, *29*, 5090–5103. [[CrossRef](#)]
23. Pania, D. Dissolution of Hematite in Acidic Oxalate Solutions: The Effect of Ferrous Ions Addition. *Hydrometallurgy* **1996**, *43*, 219–230. [[CrossRef](#)]
24. Reklaitis, G. *Introduction to Material and Energy Balances*, 1st ed.; John Wiley: New York, NY, USA, 1991; ISBN 978-0-471-04131-3.
25. Curtiss, L.A.; Raghavachari, K.; Redfern, P.C.; Rassolov, V.; Pople, J.A. Gaussian-3 (G3) Theory for Molecules Containing First and Second-Row Atoms. *J. Chem. Phys.* **1998**, *109*, 7764–7776. [[CrossRef](#)]
26. Curtiss, L.A.; Redfern, P.C.; Raghavachari, K. Gaussian-4 Theory. *J. Chem. Phys.* **2007**, *126*, 084108. [[CrossRef](#)]
27. Zuluaga, J. *Instalación de Gaussian en un Cluster Rocks*; Universidad de Antioquia: Medellín, Colombia, 2006.
28. Patel, A.M.; Nørskov, J.K.; Persson, K.A.; Montoya, J.H. Efficient Pourbaix Diagrams of Many-Element Compounds. *Phys. Chem. Chem. Phys.* **2019**, *21*, 25323–25327. [[CrossRef](#)]
29. Lema, J.M.; Cameselle, C.; Ricart, M.T.; Nu, M.J. Iron Removal from Kaolin. Comparison between “in Situ” and “Two-Stage” Bioleaching Processes. *Hydrometallurgy* **2003**, *68*, 97–105.
30. Lee, S.; Tran, T.; Park, Y.; Kim, S.; Kim, M. Study on the Kinetics of Iron Oxide Leaching by Oxalic Acid. *Int. J. Miner. Process.* **2006**, *80*, 144–152. [[CrossRef](#)]
31. Deng, B.; Wang, B.; Su, S.; Ding, S.; Sun, W. Recovery of Iron from Pyrolusite Leaching Slag by a Lab-Scale Circulation Process of Oxalic Acid Leaching and Ultraviolet Irradiation. *Metals* **2017**, *8*, 8. [[CrossRef](#)]
32. Ocampo-López, C. *Estudio Termodinámico de Remoción Biotecnológica de Hierro Presente en Caolín*; Universidad Pontificia Bolivariana: Medellín, Colombia, 2011.
33. Vincze, L.; Papp, S. Individual Quantum Yields of $\text{Fe}^{3+}\text{OX}_n^{2-}\text{H}_m^+$ Complexes in Aqueous Acidic Solutions ($\text{OX}^{2-} \equiv \text{C}_2\text{O}_4^{2-}$, $n = 1-3$, $m = 0, 1$). *J. Photochem.* **1987**, *36*, 289–296. [[CrossRef](#)]
34. Bourdoiseau, J.A.; Sabot, R.; Jeannin, M.; Termemil, F.; Refait, P. Determination of Standard Gibbs Free Energy of Formation of Green Rusts and Its Application to the Fe(II–III) Hydroxy-Oxalate. *Colloids Surf. A Physicochem. Eng. Asp.* **2012**, *410*, 72–80. [[CrossRef](#)]
35. Uchimiya, M.; Stone, A.T. Redox Reactions between Iron and Quinones: Thermodynamic Constraints. *Geochim. Cosmochim. Acta* **2006**, *70*, 1388–1401. [[CrossRef](#)]
36. Refait, P.; Bon, C.; Simon, L.; Bourrié, G.; Trolard, F.; Bessière, J.; Génin, J.-M.R. Chemical Composition and Gibbs Standard Free Energy of Formation of Fe(II)-Fe(III) Hydroxysulphate Green Rust and Fe(II) Hydroxide. *Clay Miner.* **1999**, *34*, 499–510. [[CrossRef](#)]
37. Xu, N.; Gao, Y. Characterization of Hematite Dissolution Affected by Oxalate Coating, Kinetics and PH. *Appl. Geochem.* **2008**, *23*, 783–793. [[CrossRef](#)]